

Simulation of the spiral wound RO membranes deformation under operating conditions

S.A. Avlonitis^{a*}, D.G. Pavlou^b, S. Skourtis^a

^aLaboratory of Production, Process and Environmental Engineering, ^bLaboratory of Engineering Structures and Mechanics, Technological Education Institute of Halkida, (T.E.I.-Halkidas), 34400 Psahna Evia, Greece
Tel. +30 6937206502; Fax +30 2228099664; email: savlon@teihal.gr

Received 11 February 2010; Accepted in revised form 25 July 2010

ABSTRACT

A mathematical model for the simulation of the deformation of the spiral wound reverse osmosis (RO) membranes in real operating conditions for seawater was developed. A simple analytical equation for the trans-membrane pressure was used and a mathematical procedure was applied to determine the membrane compactions. The derived mathematical model can be considered as a tool to give a detailed picture of the membrane deformation in real operating conditions, in order to relate the membrane compaction with the water flux decline. The estimation of the 2D compaction is based on the modeling of the composite membrane using the theory of a plate on an elastic substrate. Results indicated that the compaction of both composite membrane layers is varying smoothly along the membrane surface. The maximum compaction of the active bi-material polyamide-polysulfone on top of the membrane is located at the point $(x, y) = (0 \text{ cm}, 117 \text{ cm})$ having value $w_{1\text{max}} \approx 0.1 \mu\text{m}$ while the maximum compaction of polyester sub-layer is $w_{2\text{max}} \approx 16 \mu\text{m}$ taking place at the interior point $(x, y) = (29 \text{ cm}, 82 \text{ cm})$ for the 8" RO membrane modules.

Keywords: RO membranes deformation; Plate on elastic foundation; Composite membranes

1. Introduction

The compaction of reverse osmosis (RO) membranes has a significant effect on the membrane performance causing a decrease in the water permeation rate. For seawater RO membranes these effects are more important taking into account the high operating pressures. These deformation and compaction effects have been well established in the literature for the pressure driven application of desalination [1–4]. The water flux decline has been investigated for cellulose acetate membranes by Mashiko et al. [5]. It is well established that this effect is due to compaction of the dense and/or support layer. This

compaction phenomenon has been explained in several studies [6,7]. The compaction of composite membranes is expected to be different for the thin active layer and the relative thick supporting substrate because they are made from different materials with different elastic properties. The FilmTec composite membranes consist of three layers. These are: a polyester support web, a microporous polysulfone interlayer, and an ultra thin polyamide barrier layer on the top surface [8]. Each layer is tailored to specific requirements. A schematic diagram of the membrane is shown in Fig. 1. The active membrane layer with the rejection properties has a very small thickness of $0.2 \mu\text{m}$. The major structural support of the membrane is provided by the non-woven web, $100 \mu\text{m}$ thick, which has been used to produce a hard, smooth surface free of

* Corresponding author.

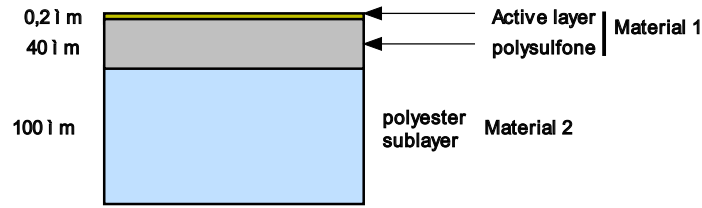


Fig. 1. Schematic cross-section of a FILMTEC thin film composite membrane.

loose fibres. Since the polyester web is too irregular and porous to provide a proper substrate for the salt barrier layer, a microporous layer of engineering plastic (polysulfone), 40 μm thick, is cast onto the surface of the web. The combination of the polyester web and the polysulfone layer has been optimized for high water permeability at high pressure.

In real operating environment the RO seawater membranes experience high loads due to the high pressure operating conditions. The applied pressure is different at each point on the membrane surface. A mathematical model, which has been developed to describe the RO membrane performance by Avlonitis et al. [9], can be used to estimate the pressure distribution on the membrane surface and consequently the membrane compaction and deformation.

The purpose of this work is to develop an explicit procedure to determine the compaction of the total structure of the composite membrane for seawater RO membranes under real operating conditions.

2. Theory

2.1. The flow model

The flows of the seawater and water in the feed and permeate channels respectively in RO spiral wound membrane modules can be approximated as flow in

a rectangular porous channel with elastic walls from aromatic polyamides composite membranes (Fig. 2). A complete list of the assumptions used in the modelling of the spiral wound modules performance for the derivation of the effective pressure at steady state conditions in this paper, is given in Table 1.

A detailed presentation and the experimental validation of the mathematical model for the performance of the RO membranes has been presented elsewhere [9–11]. The proposed mathematical model in this work has been also used and confirmed by others [12]. The flow conditions in these flat channels are changing at every point (x,y). One of the parameters calculated by the used mathematical model is the effective pressure. This is the actual deformation pressure for the membrane sheets and is given by Eq. (6):

$$\Delta P_{ef}(x,y) = k \frac{\Delta P - c_f \omega + \frac{c_f u_f k_{fb} \mu}{f} \ln \frac{c_f}{c_f + fx} - \omega fx}{[k + k_1 \omega (c_f + fx)]} \times \frac{\cosh \frac{y}{q}}{\cosh \frac{w}{q}} \tag{6}$$

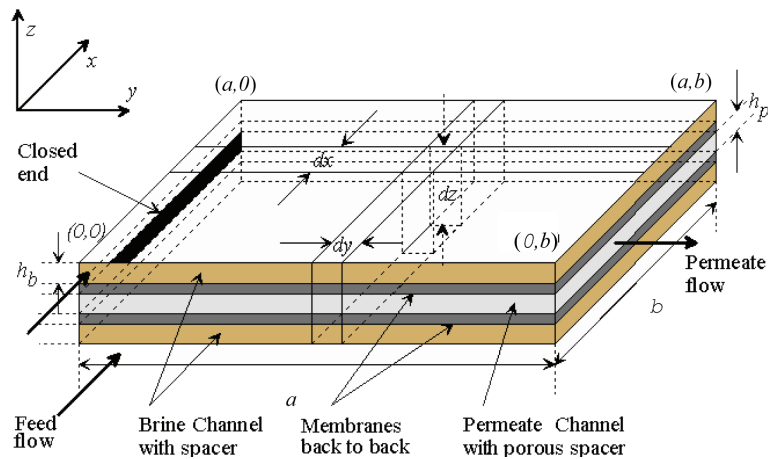


Fig. 2. Unwound spiral wound RO membrane module.

Table 1
Assumptions for the 2-dimension flow calculations

1. Validity of Darcy's law for permeate and brine channel.
2. Validity of solution-diffusion model, for the transport of water through the membrane. No flow restrictions for the locally produced permeate in the porous substructure of the composite membrane.
3. Immediate and complete mixing of the locally produced permeate water with the bulk flow in the permeate channel.
4. The permeate concentration has been neglected in comparison to the feed concentration.
5. Membrane modules are made up of flat channels, with constant geometrical shape (Fig. 1).
6. Constant fluid properties.
7. Negligible components of brine and permeate velocities along the y (tangential) and x (axial) axis respectively.
8. Negligible diffusive mass transport along the x and y direction in both channels. This means that the flux through the membrane due to diffusion is much smaller to the flux due to convection. The driving force for the water transport is the effective pressure across the membrane.
9. The brine concentration varies linearly with the distance L , in the axial direction.

$$c_b(x) = c_f + fx \quad (1)$$

where

$$f = \frac{c_b(L) - c_f}{L} \quad (2)$$

The value of f is an indication of the recovery ratio R .

10. Validity of the thin film theory, with the approximation which is given by Eq. (3).

$$c_{bw} = c_b \left(1 + \frac{J}{k} \right) \quad (3)$$

11. A constant mass transfer coefficient, given by Eq. (4) [9,10]

$$\text{Sh} = 0.63 \times \text{Sc}^{0.17} \times \text{Re}_f^{0.40} \times \left[\frac{c_f}{\rho} \right]^{-0.77} \times \left[\frac{P_f}{P_o} \right]^{-0.55} \quad (4)$$

12. Osmotic pressure proportional to the concentration [Eq. (5)]

$$\pi = \omega \times c \quad (5)$$

2.2. The mechanical model

As the active layer is ultrathin (0.2 μm), the influence of its rigidity on the pressure distribution of the polysulfone (40 μm) can be neglected. Therefore, from the view point of theory of elasticity, the bi-materials of polyamide and polysulfone can be considered as a uniform material (material 1). Furthermore, as the pressure on polyester sub-layer (material 2) is transferred through the material 1, the mechanical properties (rigidity) of material 1 influences the active pressure distribution in the surface of material 2. Therefore, the compaction of material 2 is going to be estimated separately.

2.2.1. Material 1 (polyamide and polysulfone layers)

According to the Hooke's law the deformation of material 1 can be estimated by the formula:

$$\varepsilon_1(x, y) = \frac{1}{E_1} \sigma_1(x, y) \quad (7)$$

where $\varepsilon_1(x, y)$ is the strain distribution, E_1 is the modulus of elasticity and $\sigma_1(x, y)$ is the stress distribution on the surface of material 1, i.e.

$$\sigma_1(x, y) = \Delta P_{\text{eff}}(x, y) \quad (8)$$

Taking into account the following relation between the compaction w_1 of the material 1 with its initial thickness h_1 , the compaction distribution of material 1 can be estimated as:

$$\frac{w_1(x, y)}{h_1} = \frac{1}{E_1} \Delta P_{\text{eff}}(x, y) \Rightarrow w_1(x, y) = \frac{h_1}{E_1} \Delta P_{\text{eff}}(x, y) \quad (9)$$

Using the values (see Appendix and Fig. 1) $E_1 = 1 \times 10^5 \text{ N/cm}^2$, $h_1 = 40.2 \times 10^{-4} \text{ cm}$ as well as the pressure model

given by Eq. (6), the graphical representation of compaction distribution of material 1 can be obtained. Eq. (9) shows that the compaction distribution for material 1 is directly proportional to the pressure distribution. The maximum compaction has the value of $w_{1max} = 9.5 \times 10^{-6}$ cm (i.e. $\approx 0.1 \mu\text{m}$) and it is acting in the location $(x, y) = (0 \text{ cm}, 117 \text{ cm})$.

2.2.2. Material 2 (polyester sub-layer)

The compaction distribution $w_2(x,y)$ of material 2 can be approximated using the theory of a plate on an elastic substrate (Fig. 3).

For this model, the following assumptions were made:

1. The material 1 (the polysulfone and the active membrane layer) should be treated as a plate resting on elastic substrate.
2. The polyester sublayer (material 2) should be treated as the elastic substrate.
3. Using Winkler's assumption [13,14], the compaction of the material 2 at any point (x,y) can be considered identical to the pressure acting on the interface between the two layers, $q(x, y) \neq \Delta P_{eff}(x, y)$.
4. The material 1 is perfectly bonded to material 2.
5. The mechanical behavior of both materials should be considered perfectly elastic.
6. The deformation of the material 1 can be considered independent from the polyester support. Therefore, the polysulfone layer should be considered as a plate with all four edges simply supported.

2.3. The mathematical model

A differential equation describing the deflection $w_2(x,y)$ of a rectangular plate on an elastic substrate is given [e.g 15] by:

$$\frac{\partial^4 w_2(x, y)}{\partial x^4} + 2 \frac{\partial^4 w_2(x, y)}{\partial x^2 \partial y^2} + \frac{\partial^4 w_2(x, y)}{\partial y^4} + \frac{k}{D} w_2(x, y) = \frac{\Delta P_{eff}(x, y)}{D} \tag{10}$$

where k is the modulus of the elastic substrate which can be approximated [15] by the rule

$$k = \frac{E_2}{2(1-\nu_2^2)} \tag{11}$$

while D is the flexural rigidity of material 1 given by

$$D = \frac{E_1 h_1^3}{12(1-\nu_1^2)} \tag{12}$$

In the above equations, E_j, ν_j, h_j are the Young modulus, Poisson's ratio and thickness of material j respectively. Taking the coordinate axes as shown in Fig. 2, the Navier solution [15] of Eq. (10) can be written:

$$w_2(x, y) = \sum_{m=1}^{\infty} \sum_{n=1}^{\infty} A_{mn} \sin \frac{m\pi x}{a} \sin \frac{n\pi y}{b} \tag{13}$$

where a, b are the dimensions of the rectangular plate, while A_{mn} are unknown coefficients.

In order to calculate the above unknown coefficients A_{mn} , the following Fourier series can be used to represent the pressure distribution $\Delta P_{eff}(x,y)$:

$$\Delta P_{eff}(x, y) = \sum_{m=1}^{\infty} \sum_{n=1}^{\infty} a_{mn} \sin \frac{m\pi x}{a} \sin \frac{n\pi y}{b} \tag{14}$$

Substituting Eqs. (13) and (14) into the differential Eq. (10), Eq. (15) can be obtained:

$$A_{mn} = \frac{a_{mn}}{\pi^4 D \left(\frac{m^2}{a^2} + \frac{n^2}{b^2} \right)^2 + k} \tag{15}$$

Then, the required solution of the compaction distribution $w_2(x,y)$ of the material 2 can be approximated by the following equation:

$$w_2(x, y) = \sum_{m=1}^{\infty} \sum_{n=1}^{\infty} \frac{a_{mn}}{\pi^4 D \left(\frac{m^2}{a^2} + \frac{n^2}{b^2} \right)^2 + k} \sin \frac{m\pi x}{a} \sin \frac{n\pi y}{b} \tag{16}$$

2.4. Numerical solution for compaction distribution of material 2

Taking into account the fact that the pressure distribution $\Delta P_{eff}(x,y)$ is given by Eq. (6), the expansion of

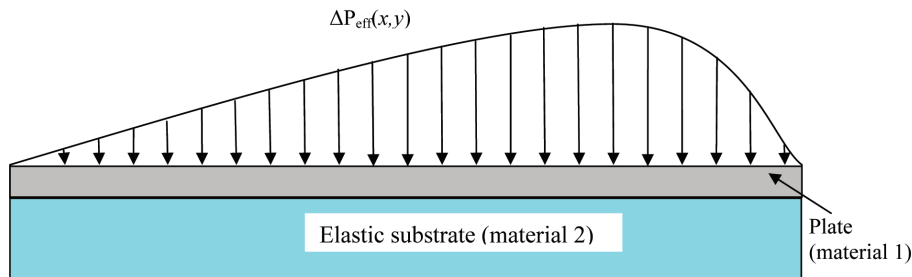


Fig. 3. The mechanical model.

the Fourier series in Eq. (14) can be represented by the following equation:

$$a_{mm} = \frac{4}{ab} \int_0^a \int_0^b \Delta P_{eff}(x, y) \sin \frac{m\pi x}{a} \sin \frac{n\pi y}{b} dx dy \quad (17)$$

where a, b are the plate's dimensions given in the Appendix (i.e. $a = 85$ cm and $b = 117$ cm).

Furthermore, taking into account that $E_1 = 1 \times 10^5$ N/cm², $E_2 = 2.54 \times 10^5$ N/cm², $\nu_1 = \nu_2 = 0.3$, $h_1 = 0.014$ cm (see Appendix), the values of modulus of elastic substrate k and flexural rigidity D can be obtained with the aid of Eqs. (11) and (12). Therefore, $k = 139560$ N/cm² and $D = 0.025$ N/cm².

3. Numerical algorithm and results

A graphic representation of Eq. (6) is illustrated in Fig. 4 for the 8" SW30HR380 membrane modules made by FilmTec.

It is apparent that a variable effective pressure with a maximum pressure difference of more than 5 bar is applied on the membrane surface.

A similar graph can be obtained for the compaction of material 1 by the use of Eq. (9), which is illustrated in Fig. 5.

The compaction of materials 2 was evaluated using Eqs. (6), (16), (17) as well as data from the membrane dimensions $a = 85$ cm and $b = 117$ cm and the values for k and D . The equations were solved using the commercial software package "Mathematica" [16].

Convergence of the summation in Eq. (15) required 30 terms for both n and m for the Fourier series in Eq. (15). Fig. 6 shows the compaction distribution obtained for material 2. In this figure, the graphical excursions obtained at the corners are due to a mathematical discontinuity.

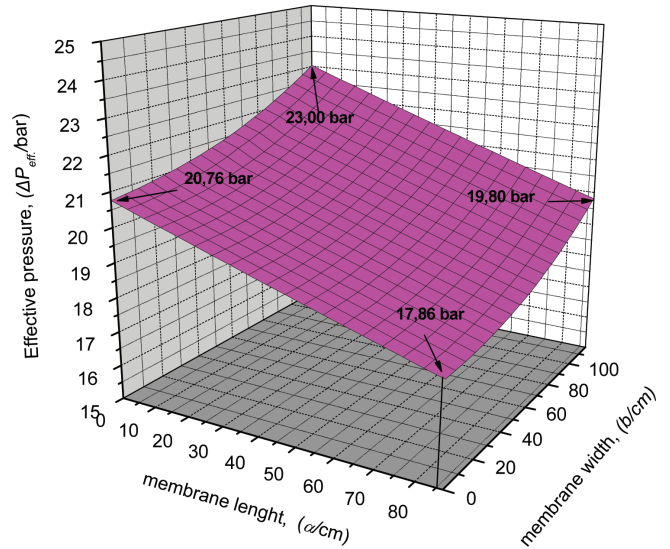


Fig. 4. Membrane effective pressure profile for $c_f = 40$ kg/m³, $u_f = 0,267$ m/s, at 20°C and 60 bar.

4. Discussion

Comparing the results shown in Figs. 4, 5 and 6, the following comments can be made:

1. The minimum applied effective pressure is applied at the point (85 cm, 0). At this point the feed pressure has been reduced due to the increasing osmotic pressure and pressure losses, while the permeate pressure has the maximum value at the closed end of the membrane envelope.
2. The maximum applied effective pressure is applied at the point (0, 117 cm). At this point the permeate pres-

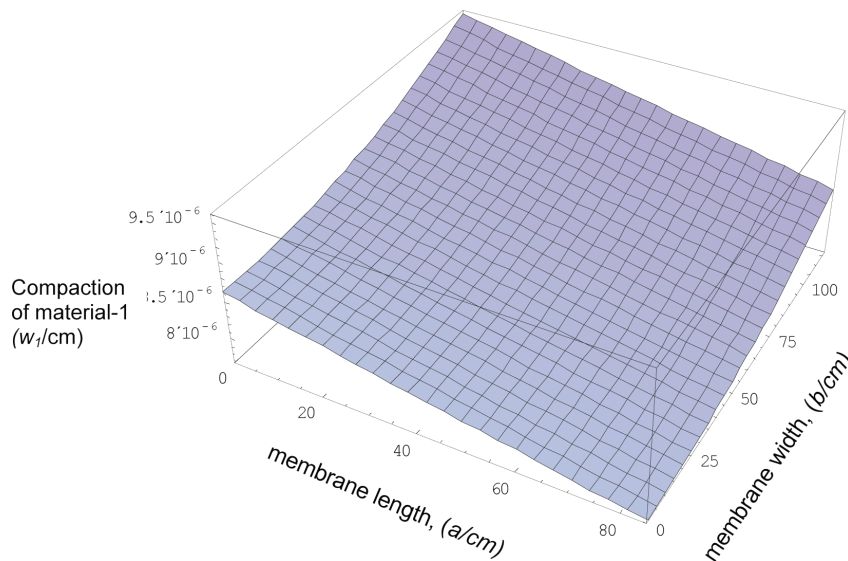


Fig. 5. RO membrane's material 1 compaction distribution.

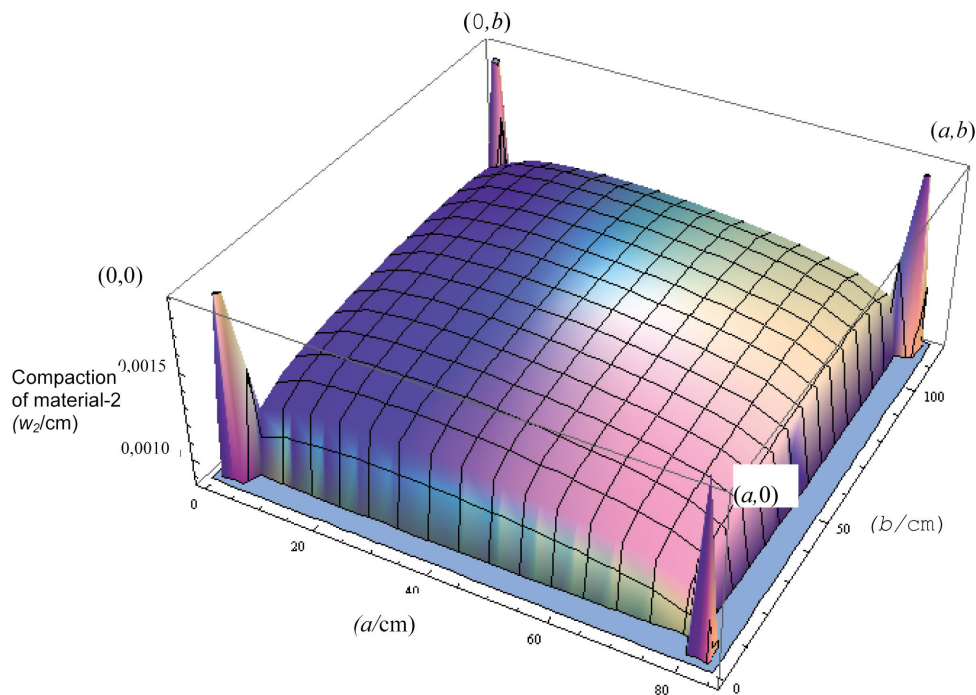


Fig. 6. Compaction distribution of material 2 of the RO membrane.

- sure and the osmotic pressure have their minimum values and the feed pressure is maximum.
- The surface of the deformed membrane is curved. The compaction distribution is smooth.
 - The shape of compaction distribution w_1 of material 1 is identical with the shape of pressure distribution $\Delta P_{\text{eff}}(x, y)$,
 - The maximum compaction of material 1 is located at the point $(x, y) = (0 \text{ cm}, 117 \text{ cm})$ having value $w_{1\text{max}} = 9.5 \times 10^{-6} \text{ cm}$ (i.e. $\approx 0.1 \mu\text{m}$). Hence, the mechanical compaction of the material 1, which includes the active membrane layer, is very low. At this point it is impossible to find the compaction on the very thin active layer. No conclusion can be made about the a percentage the compaction of the active layer in order to explain the water production decline of the RO membranes, which is taken palace in the long term.
 - The maximum compaction of material 2 is $w_{2\text{max}} = 0.0016 \text{ cm}$ representing 13.35% of the thickness of the polyester layer.
 - Although the maximum pressure is located at the point $(x, y) = (0, 117 \text{ cm})$ at the corner of the exterior perimeter of the membrane, the maximum compaction is located at the interior point $(x, y) = (29 \text{ cm}, 82 \text{ cm})$.

Symbols

- A — Cross sectional area, m^2
 α_{mn} — Coefficients of Fourier series
 a — Membrane length (axial), m

- b — Membrane width (tangential), m
 c — Concentration, kg m^{-3}
 D — Flexural rigidity of material 1
 d — Inner diameter, m
 d_h — Hydraulic diameter, m
 e — Wall thickness, m
 E — Young's module, N m^{-2}
 E_j — Modulus of elasticity of material j , N cm^2
 f — Constant defined by Eq. (2), kg m^{-4}
 ΔP_{eff} — Driving pressure, bar
 ΔP — Pressure difference given by $(P_f(0, w) - P_p(0, w))$, bar
 h — Height, m
 h_j — Thickness of material j
 J — Average volumetric flux, m s^{-1}
 K — Bulk module, N m^{-1}
 k — Mass transfer coefficient, m s^{-1}
 k — Modulus of elastic sub-grade
 k_1 — Water permeability coefficient, $\text{m s}^{-1} \text{bar}^{-1}$
 k_f — Friction parameter, m^{-2}
 P — Pressure, Pa
 P_f — Applied pressure at the inlet of the pressure vessel, Pa
 P^o — Constant (10^5), Pa
 q — Constant for a given membrane and temperature, defined by $q = \sqrt{\frac{h_p}{2k_1 k_{fp} \mu}}$, m
 Re — Reynolds number ($\text{Re} = huQ/\mu$)
 Sc — Schmidt number ($\text{Sc} = \mu/\rho D$)

- Sh — Sherwood number ($Sh = khb/D$)
 u — Velocity, m/s
 x — Coordinate along the membrane length, m
 w_1 — Compaction distribution of material 1, cm
 w_2 — Compaction distribution of material 2, cm
 y — Coordinate along the membrane width, m

Greek

- μ — Viscosity, $\text{kg m}^{-1} \text{s}^{-1}$
 ν_j — Poisson ratio of material j
 Π — Perimeter, m
 π — Osmotic pressure, Pa
 ρ — Density, kg/m^3
 ω — Osmotic pressure coefficient, N m kg^{-1}

Subscripts

- b — Brine
 eff — Effective
 f — Feed
 m — Membrane
 p — Permeate

References

- [1] J.L. Bert, Membrane compaction: a theoretical and experimental explanation, *J. Polym. Sci., B Polym. Lett.*, 7 (1969) 685.
 [2] W. Pusch and G. Mossa, Influence of pressure and/or pressure differential on membrane permeability, *Desalination*, 24 (1978) 39.
 [3] P.F. Fuls, M.P. Dell and I.A. Pearson, Non-linear flow through compressible membranes and its relation to osmotic pressure, *J. Membr. Sci.*, 66 (1992) 37.
 [4] B.J. Rudie, T.A. Torgrimson and D.D. Spatz, Reverse osmosis and ultrafiltration membrane compaction and fouling studies using ultrafiltration pre-treatment, *ACS Symp. Ser.*, 281 (1985) 403.
 [5] Y. Mashiko, Y. Kurokawa and S. Saito, Initial flux decline of the cellulose acetate butylate membranes with time under RO performance, *Desalination*, 48 (1983) 147–160.
 [6] Y. Kurokawa, M. Kurashige and N. Yui, A viscoelastic model for initial flux decline through reverse osmosis membranes, *Desalination*, 52 (1984) 9.
 [7] H. Ohya, An expression method of compaction effects on reverse osmosis membranes at high pressure operation, *Desalination*, 26 (1978) 163–174.
 [8] FilmTec Technical Manual, 2007.
 [9] S.A. Avlonitis, W.T. Hanbury and M.B. Boudinar, Spiral wound modules performance. An analytical solution: Part II, *Desalination*, 89 (1993) 227–246.
 [10] S.A. Avlonitis, M. Pappas and K. Moutesidis, A unified model for the detailed investigation of membrane modules and RO plants performance, *Desalination*, 203 (2007) 218–228.
 [11] S. Avlonitis and D. Papanikas, Flow parameters profiles in cross-flow of a two component fluid through semipermeable membranes, *Separ. Sci. Technol.*, 32(5) (1997) 939–950.
 [12] F. Mahbub, M.N.A. Hawlader and A.S. Mujumdar, Combined water and power plant (CWPP) — a novel desalination technology, *Desal. Wat. Treat.*, 5 (2009) 172–177.
 [13] J. Jaeger, *New Solutions in Contact Mechanics*, WIT Press, 2005.
 [14] D.G. Pavlou, N.V. Vlachakis and M.G. Pavlou, An analytical solution of the annular plate on elastic foundation, *Struct. Eng. Mechanics*, 20(2) (2005) 209–224.
 [15] S.P. Timoshenko and S. Woinowsky-Krieger, *Theory of Plates and Shells*, McGraw Hill, 1959.
 [16] Wolfram Research Ltd., *Mathematica for Microsoft Windows*, Version 4.1.1, 2000.

Appendix

Dimensions of the 8'' SW30HR380 modules and the values of the constants for the membrane performance.

Permeate channel height (mm)	$h_p = 0.52$
Brine channel height (mm)	$h_b = 0.84$
Total membrane height (mm)	$h_m = 0.14$
Total membrane length (cm)	$a_2 = 96.50$
Active membrane length (cm)	$a = 85$
Total membrane width (cm)	$b_2 = 134$
Active membrane width (cm)	$b = 117$
Active membrane area (m^2)	$A = 35.00$
Water permeability coefficient ($\text{cm}^{-1} \text{bar}^{-1}$)	$k_1 = 4.2 \times 10^{-5}$
Mass transfer coefficient (cm/s)	$k = 2.7 \times 10^{-3}$
Permeate friction parameter (cm^{-2})	$k_p = 1,100,000$
Permeate friction parameter (cm^{-2})	$k'_p = 309 \times \text{Re}_f^{0.83}$
Module of elasticity of material 1 (N/cm^2)	$E_1 = 1 \times 10^5$
Module of elasticity of material 2 (N/cm^2)	$E_2 = 2.54 \times 10^5$
Poisson's ratio of material 1	$\nu_1 = 0.3$
Poisson's ratio of material 2	$\nu_2 = 0.3$
Thickness of material 1	$h_1 = 0.014 \text{ cm}$
Osmotic pressure coefficient ($\text{bar cm}^3 \text{g}^{-1}$)	$\omega = 728$
Number of leaves in 8'' SW30HR380	$N = 13$